Flow-noise and turbulence in two tidal channels

Christopher Bassett

Department of Mechanical Engineering, University of Washington, Seattle, Stevens Way, Box 352600, Seattle, WA 98165

Jim Thomson

Applied Physics Laboratory, University of Washington, Seattle, 1013 NE 40th St., Box 355640, Seattle, WA 98105-6698

Peter Dahl

Applied Physics Laboratory, University of Washington, Seattle, 1013 NE 40th St., Box 355640, Seattle, WA 98105-6698

Brian Polagye

Department of Mechanical Engineering, University of Washington, Seattle, Stevens Way, Box 352600, Seattle, WA 98165

1 Abstract

Flow-noise resulting from oceanic turbulence and interactions with pressure-sensitive transducers can interfere with ambient noise measurements. This noise source is particularly important in low-frequency measurements (< 100 Hz) and in highly turbulent environments such as tidal channels. This work presents measurements made in the Chacao Channel, Chile and in Admiralty Inlet, Puget Sound, Washington. In both environments, peak currents exceed 3 m s^{-1} and pressure spectral densities attributed to flow-noise are observed at frequencies up to 500 Hz. At 20 Hz, flow-noise exceeds mean slack noise levels by more than 50 dB. Two semi-empirical flow-noise models are developed and applied to predict flow-noise at frequencies from 20-500 Hz using measurements of current velocity and turbulence. The first model directly applies mean velocity and turbulence spectra while the second model relies on scaling arguments that relate turbulent dissipation to the mean velocity. Both models, based on prior formulations for infrasonic ($f < 20$ Hz) flow-noise, agree well with observations in Chacao Channel. In Admiralty Inlet, good agreement is shown only with the model that applies mean velocity and turbulence spectra, as the measured turbulence violates the scaling assumption in the second model.

PACS numbers: 43.30.Nb, 43.28.Ra, 43.50.Cb

2 Introduction

Pressure fluctuations occur when fluid moves relative to an immersed body at high Reynolds numbers. If sufficiently large in magnitude, these fluctuations can be measured by a pressure sensitive transducer. This phenomenon, called *flow-noise* or *pseudosound*, is a result of both advected ambient turbulence and interactions with the transducer in the flow. Unlike other ambient noise sources, flow-noise does not propagate and should not be included in ambient noise statistics. In some cases, the magnitude of these pressure fluctuations is much greater than those associated with ambient noise. Although flow-noise is fundamentally a low frequency phenomenon, the range of frequencies over which flow-noise can interfere with ambient noise measurements is dependent on the intensity of turbulence and the transducer geometry.

Flow-noise in the ocean has been identified in a number of applications utilizing stationary measurement platforms. In Narragansett Bay, Rhode Island measurements in the octave band centered at 25 Hz (Willis and Dietz, 1965) and frequency bands from 40 to 100 Hz (Dietz *et al.*, 1960) were found to be strongly correlated with tidal cycles. Webb (1988) identifies infrasonic flow-noise in the bottom boundary layer. Flow-noise induced by wave orbital motion has been reported up to 500 Hz (Gobat and Grosenbaugh, 1997), and flow-noise on moored instruments in shallow water has been reported at frequencies below 50 Hz (Deane, 2000).

While flow-noise often appears in measurements, predicting its acoustic spectrum is a more difficult task. Webb (1988) and Strasberg (1979, 1985) identify and suggest models for infrasonic flow-noise based largely on scaling arguments related to the mean flow velocity. Beyond the infrasonic range ($f < 20$ Hz), there are no generalized models for flow-noise. For advected turbulence with a length scale that is small in comparison to the characteristic size of the hydrophone, phase variations across the surface of the hydrophone cause pressure fluctuations to partially cancel and increase the spectral slope of flow-noise relative to turbulence (Strasberg, 1979). This study focuses on flow-noise associated with turbulent scales that are similar to and smaller than the size of the hydrophone.

There are few published ambient noise studies in highly energetic environments, defined here as locations where turbulent kinetic energy (TKE) exceeds 0.0025 m^2 s^{-2} and mean currents in exceed of 0.5 m s^{-1}. In recent years, an interest exploiting strong currents for tidal power generation has led to ambient noise studies in such locations to understand the potential environmental impacts of power production (e.g., Polagye et al. (in revision)). One of the primary environmental concerns associated with commercial-scale tidal power extraction is the acoustic emissions from tidal turbines because of their potential to affect marine mammal behavior (Polagye *et al.*, 2011). At tidal energy sites, flow-noise presents a significant challenge to quantifying ambient noise, especially at low frequencies.

Drifting platforms are one approach to characterizing sound in high-flow environments since the relative velocity between drifters and the mean flow is small. This limits both the advection of turbulence across the transducer and turbulence shed by the transducer. However, drifter studies are labor intensive, convolve space and time, and cannot cost-effectively quantify temporal variations in sound over long time scales (e.g., hours to months). Therefore, a robust assessment of ambient noise conditions or turbine noise requires that instrumentation packages must be deployed over time periods longer than permitted by drifting studies, and thus must be exposed to strong currents.

2.1 Turbulent velocity fluctuations

Currents in tidal channels have velocity components related to deterministic tides, meteorological currents (e.g., storm surges and wave-induced currents), and turbulence (Polagye and Thomson, 2013). If meteorological currents are negligible, the current velocity can be represented as $u = \overline{u} + u'$, where $\overline{u}$ is the mean, deterministic velocity which is nearly constant over short (e.g., 5-10 minute) sample periods and u' are the turbulent velocity fluctuations. In general, u is a vector with along-channel, cross-channel, and vertical components when projected along the principal axis. Hereafter, all velocity references refer to the component projected along the principal axis of the flow.

Identification of the range of temporal and spatial scales of turbulence is critical to the interpretation of fluctuations sensed by a pressure sensitive transducer. Previous work in high-current environments identifies two important turbulent domains: the large-scale, horizontal eddies containing most of the turbulent kinetic energy, and the small-scale isotropic eddies of the inertial subrange (Thomson *et al.*, 2012). Turbulent kinetic energy is dissipated at smaller length scales (dissipation range). Kolmogorov (1941) provides the theoretical basis for the assumption of isotropic turbulence and an analysis of measurable spatial patterns in isotropic turbulence. The theoretical wavenumber spectrum in the inertial subrange is written as

$$S_u(k) \;=\; a\epsilon^{2/3}k^{-5/3}, \tag{1}$$

where $S_u(k)$ is the turbulent spectrum, ϵ is the dissipation rate of turbulent kinetic energy, a is a constant, and k is the spatial wavenumber of the turbulence scales. Invoking Taylor's frozen turbulence hypothesis (Taylor, 1938) and substituting the frequency for the wavenumber, the turbulence spectrum in the inertial subrange is described by

$$S_u(f) \;=\; a\epsilon^{2/3}f^{-5/3}\left(\frac{\overline{u}}{2\pi}\right)^{2/3}, \tag{2}$$

where a f is the frequency and $\overline{u}$ is the mean advected velocity.

The turbulent energy of large-scale, typically anisotropic, eddies is transferred to smaller scales, a process that continues until viscous forces damp out the fluctuations. Basic scaling arguments are used to identify the spatial and temporal scales at which turbulent fluctuations occur. The smallest turbulent scales found in the inertial subrange, the Kolmorogov microscales, are related to the viscosity and the dissipation rate of turbulent kinetic energy. The Kolmorogov length scale (η_o) is defined as

$$\eta_o = \left(\frac{\nu^3}{\epsilon}\right)^{1/4}, \tag{3}$$

where ν is the kinematic viscosity. At frequencies greater than those associated with the Kolmorogov mircoscales the spectral slope is steeper than in the inertial subrange due to preferential damping by viscosity.

2.2 Turbulent pressure fluctuations

Turbulence in the ocean can generate noise through multiple mechanisms: sound radiated by turbulence and noise resulting from the presence of a pressure sensitive transducer in the flow. Proudman (1952) and Lighthill (1952, 1954) provide a theoretical basis for the radiation of sound by turbulence. The relationships developed in these papers highlight that the sound radiation efficiency has a strong dependence on the Mach number (M^5), defined as $\overline{u}/c$, where $\overline{u}$ is the advected velocity and c is the celerity. Given the celerity of seawater (≈ 1500 m s^{-1}), the Mach number is small and sound generated by turbulence underwater is radiated inefficiently. Noise levels attributed to this radiated sound are well below typical ambient noise levels in the ocean (Wenz, 1962; Ross, 1976).

The second mechanism, pressure fluctuations associated with turbulence, cannot be measured remotely because they do not produce propagating sound waves. The non-propagating pressure fluctuations that can be locally measured are advected turbulent pressure fluctuations and fluctuations resulting from the interaction between the sensor and the turbulent flow

(Strasberg, 1979, 1985; Webb, 1988). In their analyses, Strasberg (1979, 1985) and Webb (1988) identify spectra associated with flow-noise at low frequencies (< 20 Hz) in relatively low-velocity conditions ($\overline{u} < 0.5$ m s^{-1}) without co-temporal turbulence data. These studies serve as the starting point for this analysis. In the absence of interactions between pressure fluctuations and the sensor, the wide-band pressure fluctuations are related to the velocity fluctuations according to

$$\overline{p^2} = \rho^2 \left(\overline{u'^2}\right)^2, \tag{4}$$

where $\overline{p^2}$ is the mean-square pressure fluctuation, ρ is the ambient density, and $\overline{u'^2}$ is the mean-square along-channel velocity fluctuation (Kraichnan, 1956). Strasberg (1979) hypothesized a relationship between velocity and pressure spectra,

$$S_p(f) = \rho^2 \overline{u'^2} S_u(f), \tag{5}$$

where $S_p(f)$ is the pressure variance spectrum and $S_u(f)$ is the velocity variance spectrum. While Eq. 4 can be obtained by integrating over all frequencies in Eq. 5, as Strasberg (1979) notes, there is no theoretical basis for this relationship.

Strasberg (1979, 1985) related frequency-dependent pressure fluctuations to velocity fluctuations according to

$$S_p(f) = \rho^2 \overline{u}^2 S_u(f), \tag{6}$$

where the turbulent velocity term in Eq. 5 is replaced with the mean velocity. When velocity fluctuations are advected across the sensor, the observed frequency is related to mean velocity and wavelength of the velocity fluctuation (λ) according to $f = \overline{u}/\lambda$. It is expected that a sensor in the flow will be most sensitive to turbulent scales that exceed the largest dimension

(d) of the sensor such that $fd/\overline{u} \ll 1$ is satisfied (i.e., the turbulent "gust" engulfs the entire sensor). In this regime, the observed trend (e.g., slope) of the turbulent velocity spectrum is expected to be equivalent to that in the pressure spectrum. In this study, the frequencies under consideration exceed 20 Hz and it will be shown that the associated spatial scales do not satisfy $fd/\overline{u} \ll 1$. Therefore, attenuation of the pressure signal due to partial cancelation of the pressure fluctuations is expected, which increases the slope of the spectrum in this regime. Analysis of flush-mounted hydrophones suggests the attenuation scales with the dimensionless frequency according to $(fd/\overline{u})^n$ and n is related to the hydrophone geometry (Urick, 1975).

This paper presents velocity and noise data obtained in two energetic tidal channels: the Chacao Channel, Chile and northern Admiralty Inlet, Puget Sound, Washington. At both sites, peak tidal currents exceed 3 m s^{-1}, and these strong currents produce significant flow-noise for moored transducers. Co-temporal turbulence and noise measurements from the Chacao Channel are used to develop models for flow-noise and extend previous analyses of flow-noise to higher frequencies. These models are then compared to observations from Admiralty Inlet. The following sections discuss the theoretical principles and results of the flow-noise models. Sec. 3 includes a description of the measurement sites, moorings, data acquisition systems, and signal processing methods. Sec. 4 presents the data from both sites and Sec. 5 interprets the results and discusses the implications for studies in high velocity environments.

3 Methods

3.1 Sites

Co-temporal hydrodynamic and acoustic measurements were obtained from two locations in this study: the Chacao Channel near Carelmapu, Chile and Admiralty Inlet near Port Townsend, Washington, USA. Because of large dynamic range of velocities at both sites, there are no periods with true "slack" currents throughout the water column. Here "slack" refers to periods when $\overline{u} < 0.3$ m s^{-1} at the depth of the sensor platforms.

In Chacao Channel, Chile a mooring, referred to as the Tidal Turbulence and Acoustics Mooring (TTAM), was deployed to obtain hydrodynamic and acoustic measurements at S 41° 45.75', W 73° 40.95' from February 11, 2013 to February 14, 2013 (Fig. 1a-b). The mooring was deployed at a depth of approximately 38 m from the R/V Dr. Jurgen Winter, a research vessel operated by the Universidad Austral de Chile.

By using a mooring instead of a rigid platform deployed on the seabed, measurements were taken outside of the region in which boundary layer effects are most significant without utilizing a prohibitively large and expensive platform. The TTAM, further described in Thomson *et al.* (2013), consisted of three major components: a heavy anchor ($\approx$ 1050 kg in water) to hold the mooring in place, a vane on which the instruments were mounted, and a 94 cm float ($\approx$ 317 kg of buoyancy) to hold the mooring line in tension.

The vane for mounting the instrumentation was deployed in-line between the anchor and the float 9 m above the seabed at slack water. Swivels mounted to both ends of the vane provided a passive yawing mechanism to keep the instruments aligned into the principal axis of the flow and minimized the risk of mooring components interfering with the sensors. Two acoustic Doppler velocimeters (ADVs) and two autonomous hydrophone packages were deployed on the vane. The dual-package approach provided redundancy and maintained symmetry across the vane.

The Chacao Channel, in comparison with many coastal environments in the United States, has relatively small amounts of commercial shipping traffic. Shipping vessels and cruise ships bound for Puerto Montt occasionally transited the site and three large vessels were noted during daytime hours throughout the deployment period. While large shipping traffic may operate without considering the local currents, local fishing patterns are determined by them. Local fishers leave the village prior to slack tide to dive for 40 minutes near the deployment site before retuning. The local fishing vessels were, in general, less than 10 m long and have operating air compressors for surface-supplied diving. With the exception of overnight slack tides, the acoustic signals of small vessels appeared in nearly all of the slack tide recordings.

During slack water, the spectrum levels increase to approximately 80 dB re $1\mu\text{Pa}^2\ \text{Hz}^{-1}$ at 5 kHz, which is consistent with noise from snapping shrimp (Everest *et al.*, 1948; Readhead, 1997). Above 1 kHz, there are also increases in noise levels that diverge from the expected flow-noise spectrum. Energetic sites like these with beds composed of grains smaller than 10 cm can produce significant amounts of sediment-generated noise (Bassett *et al.*, 2013). The data to confirm this noise source are not available; however, the observed increases at frequencies greater than 1 kHz during non-slack conditions are consistent with the noise that would be produced by a mobilized bed composed of pebbles and gravel (Thorne, 1985, 1986).

In Admiralty Inlet, USA, co-temporal velocity and noise measurements were obtained using autonomous instrumentation packages on a tripod deployed from the R/V Jack Robertson at 48° 09.120' N, 122° 41.152' W (depth 55 m) from February 11-21, 2011 (Fig. 1c-d). In this area, Admiralty Inlet is about 5 km wide and shipping lanes and local ferry traffic result in high densities of vessel traffic (Bassett *et al.*, 2012). This site has been the subject of acoustic studies including vessel noise (Bassett *et al.*, 2012) and sediment-generated noise (Bassett *et al.*, 2013) in addition to turbulence studies (Thomson et al., 2012; Thomson et al., 2013).

An Oceanscience (www.oceanscience.com) Sea Spider tripod with additional lead ballast was modified to allow for the deployment of a variety of instrumentation packages and recovery floats. The instruments relevant to this study, an ADV and two hydrophones, were mounted vertically on one side of the tripod. The sampling volume of the ADV and the hydrophones were vertically aligned such that they each recorded 1.05 m from the seabed. There was a horizontal separation distance of approximately 30 cm between the hydrophones. The ADV was deployed such that the sampling volume was located at the midpoint between the hydrophones.

3.2 Turbulence and mean velocity measurements

The ADVs used to measure mean current velocities and turbulence at both sites were 6 MHz Nortek Vectors. In the Chacao Channel, the ADVs sampled at 16 Hz for 300 sec every 10 min. Velocity spectra were calculated for 128 sec time windows with 50% overlap. In Admiralty Inlet the sampling frequency was 32 Hz for 256 sec every 10 min and spectra were calculated using 32 sec time windows with 50% overlap. In the case of the Chacao Channel, an x-IMU (inertial motion unit) was mounted within the ADV pressure housing. IMU data was used to remove mooring motion contamination from the velocity spectra (Thomson *et al.*, 2013). For both data sets, each sample period were projected on to the principal axis, reviewed for quality, and despiked using the phase-space method (Goring and Nikora, 2002; Mori *et al.*, 2007). ADV data were used to calculate turbulence spectra, mean velocities, and the dissipation rate. Mean current velocities were linearly interpolated to form a times series with 1-min resolution.

3.3 Acoustic measurements

In both the Chacao Channel and Admiralty Inlet, the autonomous hydrophones were Loggerhead Instruments DSG data acquisition systems equipped with Hi-Tech (HTI-96-MIN) hydrophones approximately 1.9 cm in diameter and 5 cm long. In the Chacao Channel, the hydrophones were deployed on the mooring vane at a -20° angle relative to the horizontal such that the change of angle due to drag on the mooring resulted in the hydrophones being oriented roughly lengthwise into the along-channel flow. Throughout the deployment, the systems recorded ambient noise continuously with a sampling frequency of 80 kHz. Spectra were calculated using windows with 65 636 data points ($\approx$ 0.8 sec) and a 50% overlap. Each window was tapered using a Hann window. The resulting spectra had a frequency resolution of $\Delta f = 1.22$ Hz and were truncated to only include frequencies between 0.020-25 kHz (low frequency linear limit to the hydrophone through maximum frequencies of interest). Given that each recording was 62.5 sec long, timestamps were rounded down to the nearest minute for comparison to ADV data.

The motion and vibrations of the mooring caused by strong currents and turbulence contributed to self-noise. Using a combination of manual review of the audio and visual inspection of spectrograms, the signatures of two types of self-noise produced by the mooring were identified. The first type, clanging and creaking sounds associated with floats, shackles, and mooring vane, occurred occasionally. The most easily identifiable peaks attributed to this self-noise occurred around 700 Hz although energy was present between 300-1000 Hz (Fig. 2). Even during noisy periods, these sounds were identifiable.

The second type mooring noise, attributed to mooring vibrations, appeared in spectrograms as continuous noise when current velocities exceeded 0.9 m s^{-1}. In individual recordings, these peaks appeared as a constant, lower intensity noise. Examples of these peaks are visible in Fig. 6. In the spectrum associated with current velocities from 0.9-1.2 m s^{-1} there was a notable peak around 90 Hz that shifts to higher frequencies with increases in current velocity. These peaks in the spectra were relatively narrow and adjacent frequency bands are consistent with the characteristics of flow-noise.

These noises were not removed from the recordings; instead, further analysis focuses on the characteristics of the spectra outside of these frequency bands. More specifically, the analysis of flow-noise was limited to frequencies below 500 Hz and those that didn't have peaks that regularly diverged from the expected spectrum of flow-noise. It should also be noted that these increases were not consistent with vortex shedding from the hydrophone. For example, the Strouhal number for associated with a cylinder in such flows is approximately 0.2 (Schewe, 1983), which implies a shedding frequency of 12 Hz during peak currents, was too low to explain the 90 Hz noise.

Signals from vessel traffic in the Chacao Channel was, at times, easily identifiable, particularly during slack currents. The sound produced by local fishing vessels, cruise ships, and shipping vessels resulted in increased noise levels across a broad range of frequencies. To remove these points from the data set, all data were manually reviewed for signals consistent with vessel noise. Such signal characteristics included a series of tones below 500 Hz and broadband increases up to 20 kHz that evolved on time scales consistent with the passage of a vessel – up to 30 minutes depending on the vessel type (Greene and Moore, 1995; McKenna *et al.*, 2012; Bassett *et al.*, 2012). These recordings were flagged and not included in the analysis of flow-noise. A total of 466 recordings out of a total 2959 were removed due to obvious vessel traffic. Although some of the retained recordings likely include some degree of vessel traffic, this was limited to signals with relatively low pressure spectral densities.

The same hydrophones and processing techniques were used in Admiralty Inlet with two exceptions: the hydrophones recorded 10 sec at the top of every minute and they were deployed such that the hydrophones elements were oriented vertically in the water column. Admiralty Inlet has been previously identified as a noisy environment in which vessel traffic is a significant contributor to ambient noise levels (Bassett *et al.*, 2012). To identify vessel traffic, an Automatic Identification System (AIS) receiver located near the site was used to record real-time vessel traffic. In post-processing, times when an AIS transmitting vessel was within 10 km were identified and removed from the data set. The exclusion of all instances when an AIS transmitting vessel was present within the detection range of the AIS system ($\approx$20 km) would have resulted in few data points to analyze. In addition, many small vessels do not transmit AIS data. Unlike the Chacao Channel data, manual review of the data was not used to remove vessel traffic not identified by the AIS system due to the challenges of identifying these signals in a noisy environment.

3.4 Flow-noise models

Two models relating the flow-noise pressure spectra to current velocity and turbulence are developed using observations at the Chacao Channel site, which has more favorable measurement conditions (i.e., less vessel traffic). The two models are based on the frequency-dependent relationship between velocity and pressure (Eq. 6) as given by Strasberg (1979, 1985). The first model estimates flow-noise from measured mean velocity and turbulence, while the second model estimates flow-noise on the basis of mean velocity alone.

Eq. 5 also provides a basis for the development of a model; the only difference between Eqs. 5 and 6 is that the first contains the mean-square velocity fluctuation term while the second contains a mean-velocity squared term. This results in a difference of approximately 3 orders of magnitude between the two models. Given the agreement between observed data and models based on Eq. 6, the models based on Eq. 5 are not of primary importance. The development of these models in the following sections refer forward, by necessity, to some of the results formally presented in Sec. 4.

3.4.1 Flow-noise model 1: pressure spectra derived from turbulence measurements

The first model, referred to as the "turbulence model", relates the pressure spectra to the mean velocity and turbulence spectra. A semi-empirical approach is applied to scales where the assumption that the $fd/\overline{u} \ll 1$, where d is the size of the transducer, is violated. This approach requires the quantification two terms empirically: the slope of the observed pressure spectra due to partial cancelation of pressure fluctuations over the surface of the hydrophone (m) and the frequencies at which the change in slope due to decreased sensitivity occurs. The frequency at which the transition occurs is referred to as the shoulder frequency (f_{sh}). Through the substitution of the turbulence spectrum (Eq. 2) into the relationship for the pressure and velocity spectra (Eq. 6), the velocity spectrum is converted to a pressure spectrum based on the scales of the turbulence according to

$$\tilde{S}_p(f) = \begin{cases} a\rho^2\overline{u}^2\epsilon^{2/3}f^{-5/3}\left(\frac{\overline{u}}{2\pi}\right)^{2/3}, & \text{if } f < f_{sh} \quad (7) \\ a\rho^2\overline{u}^2\epsilon^{2/3}f^{-m}\left(\frac{\overline{u}}{2\pi}\right)^{2/3}, & \text{if } f > f_{sh} \quad (8) \end{cases}$$

where the tilde denotes the model.

To determine the empirical constants (f_{sh} and m) the slopes of the observed pressure spectra are calculated from 30-70 Hz. These frequencies are chosen because below 30 Hz, the frequency response of the recording system begins to roll-off and above 70 Hz mooring self-noise and lower signal-to-noise ratios (flow-noise being the signal) reduce the method accuracy. These fits are further discussed in Sec. 4.2, but for the purpose of model development we note that the observed slope follows $f^{-3.2}$, thus $m = -3.2$. This slope is applied to Eq. 8 and the shoulder frequency is identified by iteratively adjusting this term to maximize agreement with the observed pressure spectra. The best relationship between the modeled and observed spectra occurs when

$$f_{sh} = 0.1\left(\frac{\overline{u}}{d}\right). \quad (9)$$

In other words, the sensitivity to turbulent scales decreases due to partial cancellation if these scales not at least 10 times larger than the characteristic size of the hydrophone. In this formulation, the size of the hydrophone that is applied in both models is length of the hydrophone in the direction of the along-channel flow (i.e., 5 cm in Chacao Channel and 1.9 cm in Admiralty

Inlet). The shoulder frequency is always less than the frequencies included in this study (< 20 Hz). Therefore, further development of the flow-noise model is limited to Eq. 8.

Modeled spectrum levels (in dB re 1μPa^2 Hz^{-1}) are given by

$$\tilde{S}_p(f) = 10\log_{10}\left(\frac{a\rho^2\overline{u}^2\epsilon^{2/3}f_{sh}^{-5/3}\left(\frac{\overline{u}}{2\pi}\right)^{2/3}\left(\frac{f}{f_{sh}}\right)^{-3.2}}{10^{-12}}\right), \qquad \text{if } f > f_{sh} \tag{10}$$

and the modeled pressure spectra are obtained by applying the dissipation rate, mean velocity, and water density (1024 kg m^{-3}). The modeled spectra are calculated for the same frequencies as the measured acoustic spectra.

3.4.2 Flow-noise model 2: pressure spectra derived from mean-flow

One major limitation in the development of the turbulence model is that it requires an estimate for the dissipation rate, which is more difficult to obtain in high flow environments than the mean velocity. As an alternative, turbulence scaling arguments are used to develop a flow-noise model, referred to as the "mean-flow model," based on the mean advected velocity and the slope of the pressure spectra. The first scaling argument relates the dissipation rate to the largest scales of turbulence in a flow. An estimate of the rate of transfer of energy to turbulence yields $\epsilon \propto u_{rms}^3/l$, where u_{rms} is the root-mean-square of the velocity and l is the scale of the energy containing scales (Lumley, 1983; Thorpe, 2007). The velocity is decomposed as $u = \overline{u} + u'$ and the turbulence intensity is defined as

$$I = \sigma_{u'}/\overline{u}, \tag{11}$$

where $\sigma_{u'}$ is the standard deviation. If $I^2 \ll 1$, then by the mathematical definition root-mean-square velocity, $u_{rms} \approx \overline{u}$ and

$$\epsilon \propto \frac{\overline{u}^3}{l}. \tag{12}$$

Thomson *et al.* (2012) showed that the dominant scales of the TKE in two well-mixed, energetic tidal channels to be well represented by three times the water depth, assuming the tidal elevation is small compared to the depth. Therefore, the eddy scale l in the Chacao Channel is assumed to be constant so that $\epsilon \propto \overline{u}^3$. As shown in Sec. 4.1, the observed dissipation rates are consistent with this scaling at the Chacao Channel site.

Assuming that the hydrophone-specific attenuation factor $(fd/\overline{u})^n$, combined with Eq. 6, is able to describe the flow-noise, it follows that the observed velocity and frequencies dependencies should be satisfied. Therefore, the pressure spectrum scales as

$$\tilde{S}_p(f) = \rho^2 \overline{u}^2 S_u(f) \left(\frac{fd}{\overline{u}}\right)^n . \quad (13)$$

By combining Eqs. 2 and 6 and substituting $\overline{u}^3$ for ϵ, the pressure spectrum becomes

$$\tilde{S}_p(f) = a\rho^2 \overline{u}^{14/3} f^{-5/3} \left(\frac{fd}{\overline{u}}\right)^n , \quad (14)$$

where the water depth (l) is rolled into the constant a. This is an underdetermined system in which both the $\overline{u}$ and f dependencies must be satisfied by n. A slope of $f^{-3.2}$ is identified, resulting in $n \approx -1.5$, a value that agrees well with the observed velocity dependence in the Chacao Channel. The final formulation (in Pa^2 Hz^{-1}) based on this semi-empirical approach is

$$\tilde{S}_p(f) = c\rho^2 \overline{u}^{6.1} f^{-3.2}, \quad (15)$$

where c is a constant which now represents a combination of the constant from the power fit scaling between the dissipation rate and $\overline{u}$ (including the length scale l), the prior constant (a), and the slope transition associated with the sensitivity to turbulence of different scales. Notably, the magnitude of this scalar offset is dependent, in part, on the mechanisms responsible for the production and dissipation of turbulence, which vary significantly in natural environments.

Because of this, the model's framework may be applicable to other sites where $\epsilon \propto \overline{u}^3$, but the magnitude is expected to vary. To simplify the analysis and demonstrate the effectiveness of this method, the results from Eq. 15 are regressed against the observed noise levels to identify this constant. The final, spectral form (in dB re 1μPa^2 Hz^{-1}) is

$$\tilde{S}_p(f) = b + 10\log_{10}\left(\frac{\rho^2\overline{u}^{6.1}f^{-3.2}}{10^{-12}}\right), \tag{16}$$

where b is a constant.

4 Results

4.1 Turbulence results

The measurements of turbulence and mean currents made during five-minute periods are affected by two types of mooring motion. The first, a change in the angle of the mooring line due to drag forces on the float, is related to the mean currents. During peak currents, 40° angles relative to the vertical are observed, resulting in a measurement position approximately 6 m above the bed in comparison to 9 m above the bed during slack currents (Thomson *et al.*, 2013). However, the change occurs over time scales longer than 5 minutes and along-channel currents may be obtained by correcting for orientation from the internal ADV sensor. The second type of mooring motion is caused by turbulence, and can contaminate the velocity measurements. Thomson *et al.* (2013) includes analysis of the same velocity data set and demonstrates that data can be post-processed to obtain accurate turbulence spectra, as shown on a mean-velocity bin-averaged basis in Fig. 3. The inertial subrange for isotropic turbulence, which has a $f^{-5/3}$ dependence and is used to determine the dissipation rate of TKE, is evident in all of the bin-averaged spectra. The $f^{-5/3}$ slope continues until viscous dissipation damps out the turbulent fluctuations and the flattening of the spectra at high frequencies in Fig. 3 is caused by the lower limit of the instrument's sensitivity. The peaks in the TKE spectra during low current periods are caused by low-frequency mooring oscillations. When currents exceed 0.6 m s^{-1} the amplitude of the peaks in the spectra decreases due to increased tension in the mooring line.

Consistent with scaling arguments, the dissipation rate of turbulent kinetic energy increases with the mean current velocity. Fig. 4 includes time series data for the mean current velocity and the dissipation rate. The observed current velocities range from 0 to 3 m s^{-1} on both flood and ebb tides. The dissipation rates, which are shown to scale with $\overline{u}^3$ (Fig. 5a), range from less than 10^{-5} m^2 s^{-3} around slack water to greater than 10^{-3} m^2 s^{-3} during peak currents. While the dissipation rate scales with $\overline{u}^3$ at this site, it should be noted that the scaling of turbulence is largely dependent on local features of the flow (e.g., bathymetry) so this result cannot be assumed to apply in other tidal channels (Thomson *et al.*, 2013). A time series of the theoretical maximum frequency of turbulent pressure fluctuations in the inertial subrange (Eq. 3), also included in Fig. 4c, shows microscale frequencies ranging from 100 Hz during slack currents to greater than 10 kHz during peak currents.

The mean current velocity and turbulence measurements in Admiralty Inlet, just as in the Chacao Channel, reveal a highly energetic environment with peak observed near-bed current velocities of approximately 2 m s^{-1}. Unlike the measurements in the Chacao Channel, the measurements in Admiralty Inlet are within the bottom boundary layer where a large velocity gradient is observed (Bassett *et al.*, 2013) and the dissipation rates do not scale with $\overline{u}^3$ over the entire range of $\overline{u}$ (Fig. 5b).

4.2 Acoustic results

In the Chacao Channel, slack current noise levels are relatively flat below 500 Hz with spectrum levels between 60-70 dB re 1 μPa^2 Hz^{-1}. These low current conditions provide the baseline for analyzing increases due to flow-noise. Fig. 6 includes average spectra in 0.3 m s^{-1} velocity bins. Once current velocities reach approximately 0.3 m s^{-1} an acoustic signature consistent with flow-noise begins to dominate low-frequency measurements. At 20 Hz the difference between slack current noise levels and those produced by flow-noise are 10 dB, and increases are observed up to 100 Hz. As currents increase, the noise levels at the lowest frequencies do so as well, reaching levels up to 70 dB above those during slack currents. At the same time, flow-noise is observed over a wider range of frequencies. A simple analysis based on when observed noise levels diverge from the expected "red" spectrum of flow-noise suggests that it is likely to mask other sound sources at frequencies up to 800 Hz during the strongest currents. Both the velocity-bin averaged spectra and individual spectra show that the spectral slope of the flow-noise follows a $f^{-3.2}$ dependence. As previously mentioned, the theoretical maximum frequency at which flow-noise could be measured, given these dissipation rates, exceeds 10 kHz at the site during peak currents. Although flow-noise is not observed at frequencies greater than 1 kHz at this site, it is reasonable to speculate that at a site with less other noise above 1 kHz – for example, a site without sediments (i.e., scoured bedrock) and no snapping shrimp – flow-noise could be observed at higher frequencies.

The flow-noise observed in Admiralty Inlet is comparable to that observed in the Chacao Channel. Fig. 8a includes bin-averaged noise spectra up to 200 Hz in Admiralty Inlet. During slack tide periods, observed spectrum levels are approximately 80 dB re 1μPa^2 Hz^{-1}. Flow-noise is measured at frequencies less than 30 Hz once currents exceed 0.3 m s^{-1} and at frequencies greater than 200 Hz during peak currents. Peak flow-noise levels exceed slack tide conditions by up to 50 dB at 20 Hz. The observed slopes of the pressure spectra in Admiralty Inlet are in agreement with those the Chacao Channel.

4.2.1 Model-data comparisons

In the Chacao Channel, the magnitude of the constant (b) used in the mean-flow model (Eq. 16) is 48 dB re 1μPa^2 Hz^{-1}. Physically, this constant combines both the scalar constant from the dissipation scaling and the shoulder frequency (f_{sh}). The contribution of the scalar constant for the dissipation scaling, calculated as $20log_{10}\,(1.4\ 10^{-4}/10^{-6})$, yields an offset of 43 dB. Using a typical f_{sh} of 3 Hz, a value associated with current velocities of 1.5 m s^{-1}, the spectrum shift is calculated as $10log_{10}\,(20/3)$, or 8 dB. This term can be thought of as a shift necessary to account for neglecting the consideration of the hydrophone's sensitivity to different turbulent scales in the initial model. Combining these terms leads to an offset of 51 dB, a value close to the 48 dB offset shown in Fig. 7.

A comparison of nine representative, observed pressure spectra at current velocities covering the entire dynamic range in the Chacao Channel versus modeled pressure spectra using both models are included in Fig. 7, which demonstrates that both models agree well with observed spectra over most current velocities at the site (i.e., the spectra cover current velocities from 0.3-2.7 m s^{-1}). With the exception of the 0.3 and 0.6 m s^{-1} spectra, which diverge from the expected behavior of flow noise above 100 and 200 Hz, respectively, the models show good agreement up to 500 Hz. With the exception of frequencies at which self-noise from the mooring is identified, the model typically agrees with observations to within a few decibels.

Also included in Fig. 7 are scatter plots of observed pressure spectral densities in the Chacao Channel versus modeled pressure spectral densities at five frequencies between 30 and 480 Hz. Again, generally good agreement is found between the models and the observations. In the case of the higher frequencies (240 and 480 Hz) measurements associated with the weakest currents are cut-off by the y-axis. In this regime there is poor agreement between the observations and models because flow-noise does not have a significant impact at these frequencies during low current periods. At these same frequencies, there is also less agreement during peak currents (highest pressure spectral densities), with observations always exceeding the models. These differences, which can also be seen in Figs. 7a and 7b, are also attributed to mooring noise. To quantify the performance of both models, R^2 values for the modeled versus observed spectra level for the five frequencies in Fig. 7 are determined and included in Table I. The R^2 values for both models range from 0.95 for both models at 30 Hz to less than 0.7 at 480 Hz. The decreased R^2 values at higher frequencies are attributed to lower signal-to-noise ratios at higher frequencies.

Fig. 8b includes a comparison between observed and modeled flow-noise levels in Admiralty Inlet using the turbulence model at three frequencies: 30 Hz, 60 Hz, and 120 Hz. There is good agreement between the model and observations at these frequencies but there is more scatter than the results for the Chacao Channel. The additional scatter is attributed, in part, to the shorter length of the recordings in Admiralty Inlet, which results in pressure spectra with larger uncertainties. Additionally, the acoustic recordings are much shorter than the averaging periods for the turbulence spectra and are not sufficiently long to record throughout the entire period of the largest turbulent scales at the site. In comparison to the Chacao Channel data, there is also significantly more scatter in the estimated dissipation rates at a given velocity in Admiralty Inlet (Fig. 5). Disagreement at the lowest noise levels occurs during periods of low current when flow-noise levels are below ambient levels. Other significant outliers are attributed to other sources such as vessels without AIS transponders (such as military traffic).

The mean-flow model is not a good predictor of flow-noise in Admiralty Inlet. A comparison of the observations and the mean-flow model is not included due to the poor agreement. Specifically, the observed flow-noise increases at a more rapid rate than predicted by the model. This is not surprising given the dissipation rate increases more rapidly than $\overline{u}^3$ as shown in Fig. 5b. Therefore, a critical assumption in the mean-flow model is not valid at the site.

5 Discussion

As shown in Sec. 4.2, it is necessary to consider flow-noise when quantifying low-frequency ambient noise levels in areas characterized by high turbulence and currents. While the geographic distribution of such environments is quite limited, ongoing development in these areas, as well as their importance as biological choke points, will likely lead to more acoustics studies prone to high levels of flow-noise. For example, flow-noise will exceed received levels for close-range vessel traffic (Bassett *et al.*, 2012) by 30 dB or more at frequencies less than 100 Hz.

To properly quantify propagating low-frequency noise in these environments using stationary, autonomous platforms, the development of flow-noise mitigation techniques would be beneficial. While signal processing using multiple transducers can be used to reduce or eliminate flow-noise using cross-correlation techniques (Chung, 1977; Buck and Greene, 1980), these methods are of little practical value when flow-noise exceeds ambient noise levels by more than 50 dB (i.e., signal-to-noise ratios are too low for signal processing to be effective). Flow-noise can also be partially mitigated through the use of larger transducers, which will cause pressure fluctuations to cancel more rapidly over the surface (Urick, 1975; Strasberg, 1979). However, due to the large range of length scales of turbulence in energetic tidal channels, this may also be of limited utility. Ultimately, this work demonstrates a need to develop devices that are compact (to reduce drag) and shield transducers from the flow.

The models presented here, based on the basic formulations by Strasberg (1979, 1985), show good agreement with the observed data. This data set spans a wider range of current velocities than has been previously described in the literature, with peak currents nearly one order of magnitude greater than those discussed in Strasberg (1979, 1985) and Webb (1988). In addition, the frequencies studied here extend the regime of modeled flow-noise to well beyond the infrasonic range. It is expected that different hydrophone aperture geometries would have unique values for empirical constants (e.g., m, f_{sh}), although the same scaling relations would apply. To facilitate the application of higher frequency flow-noise models, further research regarding the response of hydrophones to small-scale pressure fluctuations is needed.

Both the turbulence and mean-flow models for flow-noise pressure spectra face certain limitations in application to other sites. For example, the turbulence model requires estimates of the dissipation rate or turbulence spectra in the inertial subrange. Ideally, turbulent kinetic energy spectra would be measured in the frequency range overlapping with hydrophone measurements to allow a direct evaluation of Eq. 6. However, the low-frequency response of the hydrophones employed in this study did not overlap with the velocity measurements. As such, extrapolation based on theoretical turbulence scaling was necessary. Nonetheless, the turbulence model is shown to perform well in two energetic tidal channels. The mean-flow model, by contrast, does not require turbulence measurements but relies on scaling arguments that are not universally valid. In addition, the scalar constant for the mean-flow model is expected to be site-specific. However, when these assumptions are valid, the scaling arguments can lead to accurate predictions of flow-noise levels.

The turbulence model relates mean-velocity and dissipation rate measurements to observed flow-noise levels. The good agreement between the model and measurements suggest that flow-noise spectra could be used to estimate the dissipation rate given measurements of the mean velocity when the response of the hydrophone (f_{sh} and m) is known.

Finally, the measurements presented here suffer from self-noise contamination attributed to mooring noise. This is not surprising given the engineering challenges associated with the development of a mooring to be deployed in such a dynamic environment. Isolating connection points between different mooring components using noise dampening material is one method of reducing the self-noise, which represents only one of many engineering challenges associated with the acquisition of quality ambient noise measurements in such environments.

6 Conclusions

Measurements of ambient noise in the Chacao Channel, Chile, and Admiralty Inlet, Puget Sound, Washington, two sites where peak currents exceed 3 m s^{-1}, reveal pressure spectral densities attributed to flow-noise that exceed 135 dB re μPa^2 Hz^{-1} at 20 Hz. These peak levels can exceed ambient noise by more than 50 dB. Flow-noise is observed to frequencies greater than 500 Hz. It is found that the slope of pressure spectra attributed to flow-noise is $f^{-3.2}$, a value that is expected to depend on the geometry of the hydrophone.

Two semi-empirical models are presented for flow-noise that extend the frequency range of prior models for infrasonic flow-noise. The first model utilizes direct measurements of turbulence and mean current velocities while the second uses scaling arguments to model flow-noise only on the basis of mean currents. Unlike other flow-noise studies, the frequency ranges considered here are associated with scales of turbulence that are similar to and smaller than the hydrophone. Both models are shown to agree well with flow-noise observations over the range of current velocities observed in the Chacao Channel measurements. In the Admiralty Inlet measurements, the turbulence model also agrees well with observations. However, the dissipation rate scales differently with velocity and the mean-flow model performs poorly. The agreement between the turbulence model and two observations in these dynamic channels extends the dynamic range of flow-noise models by nearly an order of magnitude.

7 Acknowledgments

Thanks to APL-UW Field Engineers Joe Talbert and Alex deKlerk as well Rodrigo Cienfuegos and Maricarmen Guerra Paris of the Pontificia Universidad Católica in Santiago, Chile. Thanks to Eduardo Hernandez and the rest of the crew of the L/M Dr. Jurgen Winter as well as Andy Reay-Ellers, captain of the R/V Jack Robertson. Funding for collaboration and field work was provided by the Office of Naval Research - Global. Student support was provided to Christopher Bassett by National Science Foundation award number DGE-0718124.

References

Bassett, C., Polagye, B., Holt, M., and Thomson, J. (**2012**). "A vessel noise budget for Admiralty Inlet, Puget Sound, Washington (USA)," J. Acoust. Soc. Am. **132(6)**, 3706–3719.

Bassett, C., Thomson, J., and Polagye, B. (**2013**). "Sediment generated noise and bed stress in a tidal channel," J. Geophys. Res.: Oceans **118**, 2249–2265.

Buck, B. and Greene, C. (**1981**). "A two-hydrophone method of eliminating the effects of nonacoustic noise interference in measurements of infrasonic ambient noise levels," J. Acoust. Soc. Am. **68(5)**, 1306–1308.

Chung, J. (**1977**). "Rejection of flow noise using a coherence function method," J. Acoust. Soc. Am. **62(2)**, 388–395.

Deane, G. (**2000**). "Long time-base observations of surf noise," J. Acoust. Soc. Am. **107(2)**, 758–770.

Dietz, F., Hahn, J. S., and Birch, W. (**1960**). "Nonrandom associations between shallow water ambient noise and tidal phase nonrandom associations between shallow water ambient noise and tidal phase," J. Acoust. Soc. Am. **32(7)**, 915 (A).

Elgar, S., Raubenheimer, B., and Guza, R. (**2001**). "Current meter performance in the surf zone," Atmos. Oceanic Tech. **18(10)**, 1735–1746.

Everest, F., Young, R., and Johnson, M. (**1948**). "Acoustics characteristics of noise produced by snapping shrimp," J. Acoust. Soc. Am. **20(2)**, 137–142.

Gobat, J. and Grosenbaugh, M. (**1997**). "Modeling the mechanical and flow-induced noise on the Surface Suspended Acoustic Receiver," in OCEANS '97. MTS/IEEE Conference Proceedings, Volume 2, 748–775.

Goring, D. and Nikora, V. (**2002**). "Despiking acoustic Doppler velocimeter data," J. Hydraul. Eng **128(1)**, 117–126.

Greene Jr., C. R. and Moore, S. (**1995**). "Man-made noise", in *Marine Mammals and Noise*, edited by J.W. Richardson, C.R. Greene, Jr., C.I. Malme, and D.H. Thompson (Academic Press, San Diego), pp. 112–113.

Kolmogorov, A. (**1941**). "Dissipation of energy in the locally isotropic turbulence," Dokl. Akad. Nauk. SSSR. **30(1)**, 301–305.

Kraichnan, R. (**1956**). "Pressure field within homogenous anisotropic turbulence," J. Acoust. Soc. Am. **28(1)**, 64–72.

Lighthill, M. (**1952**). "On sound generated aerodynamically. I. General theory," Proc. R. Soc. Lond. **211(1107)**, 564–587.

Lighthill, M. (**1954**). "On sound generated aerodynamically. II. Turbulence as a source of sound," Proc. R. Soc. Lond. **212(1148)**, 1–32.

Lumley, J. L. and Terray, E. A. (**1983**). "Kinematics of turbulence convected by a random wave field," J. Phys. Oceanogr. **13**, 2000–2007.

McKenna, M., Ross, D., Wiggins, S., and Hildebrand, J. (**2012**). "Underwater radiated noise from modern commercial ships," J. Acoust. Soc. Am. **131(1)**, 92–103.

Mori, N., Suzuki, T., and Kakuno, S. (**2007**). "Noise of acoustic Doppler velocimeter data in bubbly flows," J. Eng. Mech. **133(1)**, 122–125.

Polagye, B., Van Cleve, B., Copping, A., Kirkendall, K. (**2011**). "Environmental effects of tidal energy development," Technical Report (U.S. Dept. Commerce, NOAA Tech. Memo. NMFS F/SPO-116), 186 p.

Polagye, B., Bassett, C., Holt, M., Wood, J., and Barr, S. (**in revision**). "A framework for detection of tidal turbine sound: A pre-installation case study for Admiralty Inlet, Puget Sound, Washington (USA)," J. Ocean. Eng.

Polagye, B. and Thomson, J. (**2013**). "Tidal energy resource characterization: methodology and field study in Admiralty Inlet, Puget Sound, US," IMechE, Part A: J. Power and Energy **227(3)**, 352–367.

Proudman, I. (**1952**). "The generation of noise by isotropic turbulence," Proc. R. Soc. Lond. **214(1)**, 119–132.

Readhead, M. (**1997**). "Snapping shrimp noise near Gladstone, Queensland," J. Acoust. Soc. Am. **101(3)**, 1718–1722.

Ross, D. (**1976**), *Mechanics of Underwater Noise*, (Permagon Press, Elmsford, New York). pp. 47–54

Schewe, G. (**1983**). “On the force fluctuations acting on a circular cylinder in crossflow from subcritical up to transcritical Reynolds numbers,” J. Fluid Mech **133**, 265–285.

Stasberg, M. (**1985**). “Hydrodynamic flow noise in hydrophones,”, in H. G. Urban (Ed.) *Adaptive Methods in Underwater Acoustics*, NATO ASI Series, (Springer, Netherlands) pp. 125–143.

Strasberg, M. (**1979**). “Nonacoustic noise interference in measurements of infrasonic ambient noise,” J. Acoust. Soc. Am. **66(5)**, 1487–1493.

Taylor, G. (**1938**). “The spectrum of turbulence,” Proc. R. Soc. Lond. **164**, 476–490.

Thomson, J., Kilcher, L., Richmond, M., Talbert, J., deKlerk, A., Polagye, B., Paris, M., and Cienfuegos, R. (**2013**). “Tidal turbulence spectra from a compliant mooring,” in Proceedings of the 1st Marine Energy Technology Symposium, Washington, D.C.

Thomson, J., Polagye, B., Durgesh, V., and Richmond, M. (**2012**). “Measurements of turbulence at two tidal energy sites in Puget Sound, WA (USA),” J. Ocean. Eng. **37(3)**, 363–374.

Thorne, P. (**1985**). “The measurement of acoustic noise generated by moving artificial sediments,” J. Acoust. Soc. Am. **78(3)**, 1013–1023.

Thorne, P. (**1986**). “Laboratory and marine measurements on the acoustic detection of sediment transport.,” J. Acoust. Soc. Am. **80(3)**, 899–910.

Thorpe, S.A. (**2007**), *An Introduction to Ocean Turbulence*, (Cambridge Univ. Press, Cambridge; New York). pp. 73

Urick, R. (**1975**), *Principles of Underwater Sound for Engineers*, (McGraw-Hill Press, New York). pp. 332–333

Webb, S. (**1988**). "Long-period acoustics and seismic measurements and ocean floor currents," J. Ocean. Eng. **13(4)**, 263–270.

Wenz, G. (**1962**). "Acoustic ambient noise in the ocean: Spectra and sources," J. Acoust. Soc. Am. **34(12)**, 1936–1956.

Willis, J. and Dietz, F. (**1965**). "Some characteristics of 25-cps shallow-water ambient noise," J. Acoust. Soc. Am. **37(1)**, 125–130.

Table I: R^2 values for both flow-noise models and the observed spectrum levels in the Chacao Channel at selected frequencies.

	Frequency (Hz)				
	30	60	120	240	480
Turbulence Model R^2	0.95	0.89	0.83	0.77	0.65
Mean-Flow Model R^2	0.95	0.87	0.83	0.80	0.68

Figure 1: (Color online) a-b). South-central Chile, the study area (red rectangle), and the deployment site (red circle). c-d). Puget Sound, the study area (red rectangle), and the deployment site (red circle).

Figure 2: A 40-second spectrogram from the Chacao Channel showing the transient signals associated with clanging and creaking noise centered around 700 Hz.

Figure 3: (Color online) Velocity-bin averaged (0.3 m s^{-1} bins) TKE spectra from the Chacao Channel show the expected $f^{-5/3}$ slope associated with isotropic turbulence. During periods with weak currents ($\overline{u} < 0.3$ m s^{-1}), there is significant mooring motion contamination. However, during these periods flow-noise has little impact on observed ambient noise levels.

Figure 4: Hydrodynamics data from the Channel Channel. a). Time series of the mean current velocity. b). Time series of the dissipation rate of turbulent kinetic energy. c). Time series of the microscale frequency.

Figure 5: Scatter plots of the dissipation rate of turbulent kinetic energy versus current velocity in the Chacao Channel (a) and Admiralty Inlet (b). In Admiralty Inlet, the scaling used in the formulation of the mean-flow model ($\epsilon \sim \overline{u}^3$) is not valid.

Figure 6: (color online) Velocity bin-averaged (0.3 m s^{-1} bins) pressure spectra from the Chacao Channel. The observed flow-noise has a $f^{-3.2}$ dependence.

Figure 7: (Color online) A comparison of observed and modeled flow-noise levels using the turbulence and mean-flow models in the Chacao Channel. a,b). Modeled and observed pressure spectra for both models. The black lines are the modeled spectra using the hydrodynamic measurements at the time of the hydrophone recordings. The range of current velocities is 0.3-2.7 m s^{-1} in 0.3 m s^{-1} increments. The ten small insets includes comparison of observed and modeled pressure spectral densities at five frequencies for the turbulence and mean-flow models. The black lines are the show the 1-1 relationship.

Figure 8: (Color online) a). Velocity-bin averaged spectra (0.3 m s^{-1} velocity bins) in Admiralty Inlet for periods with no AIS transmitting vessels with 10 km of the hydrophone. The small insets include a comparison between the modeled and observed pressure spectra in Admiralty Inlet for the turbulence model at three frequencies. The mean-flow model is not shown because ϵ does not scale with $\overline{u}^3$.

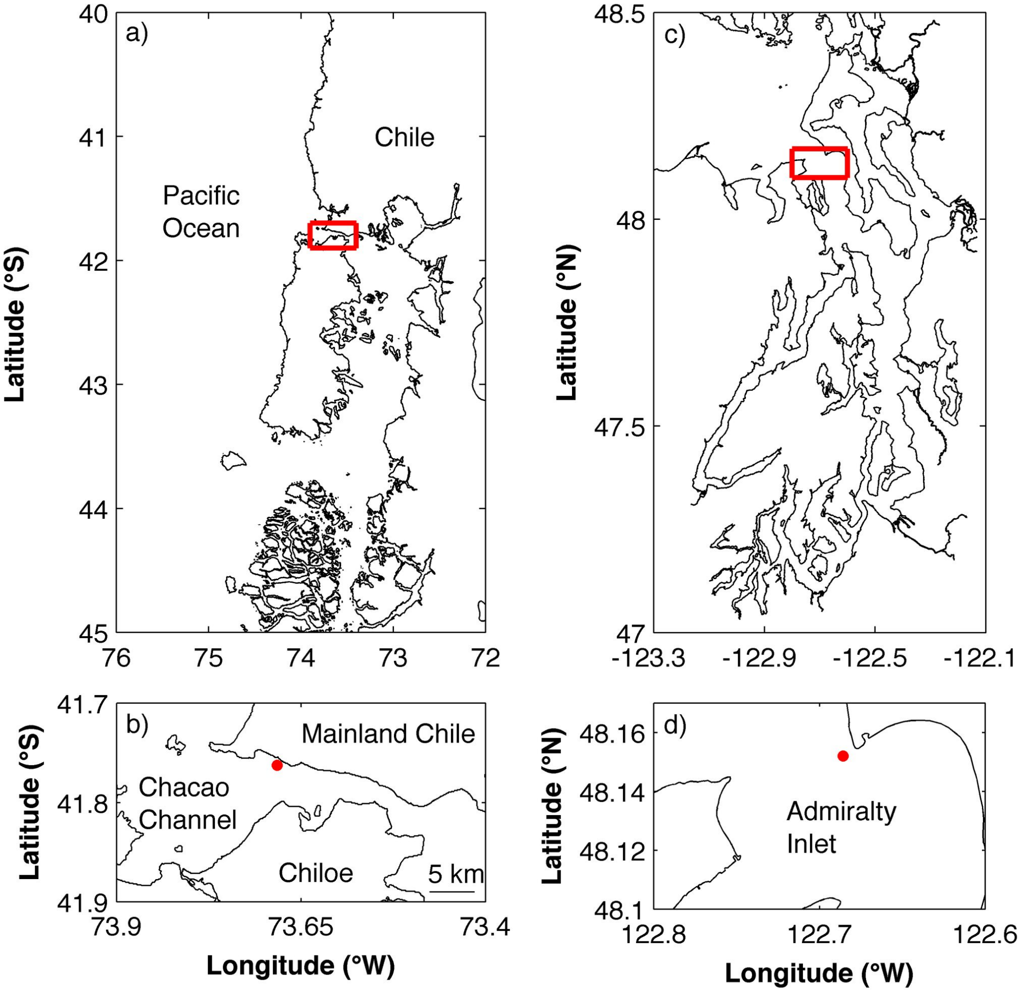
a)
Chile
Pacific Ocean
Latitude (°S)
40
41
42
43
44
45
76
75
74
73
72
b)
Mainland Chile
Chacao Channel
Chiloe
5 km
41.7
41.8
41.9
73.9
73.65
73.4
Longitude (°W)
c)
Latitude (°N)
48.5
48
47.5
47
-123.3
-122.9
-122.5
-122.1
d)
Admiralty Inlet
48.16
48.14
48.12
48.1
122.8
122.7
122.6
Longitude (°W)

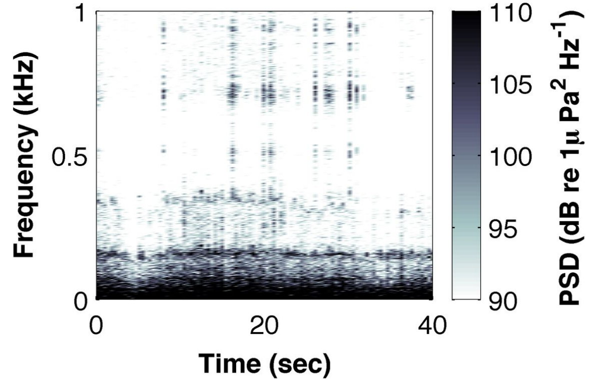

1
0.5
0
Frequency (kHz)
0
20
40
Time (sec)
110
105
100
95
90
PSD (dB re 1μ Pa² Hz⁻¹)

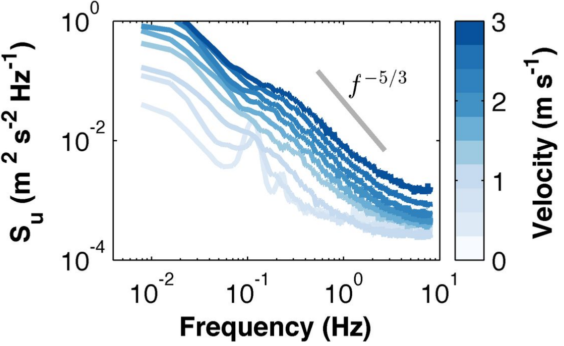

10^0
10^{-2}
10^{-4}
S_u (m^2 s^{-2} Hz^{-1})
$f^{-5/3}$
10^{-2}
10^{-1}
10^0
10^1
Frequency (Hz)
3
2
1
0
Velocity (m s^{-1})

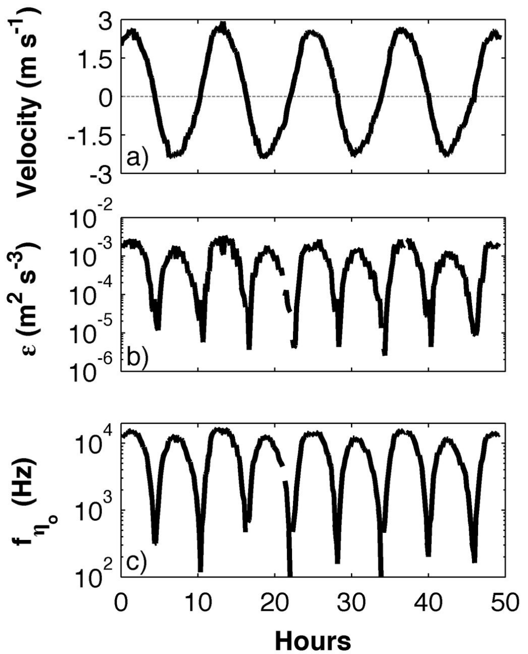

Velocity (m s-1)
3
1.5
0
-1.5
-3
a)
ε (m2 s-3)
10-2
10-3
10-4
10-5
10-6
b)
fηo (Hz)
104
103
102
c)
0
10
20
30
40
50
Hours

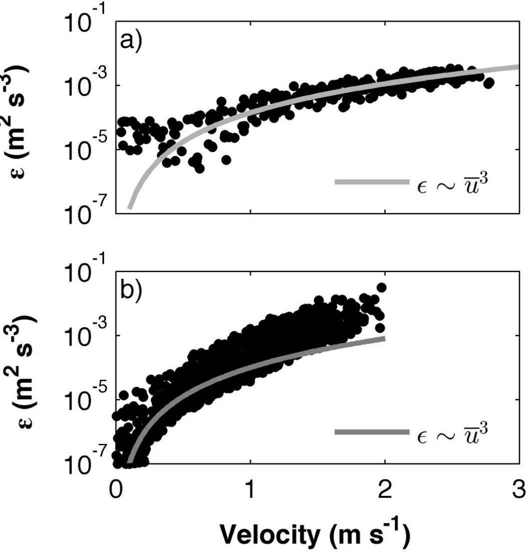

a)
b)
10^{-1}
10^{-3}
10^{-5}
10^{-7}
ε (m^2 s^{-3})
$\epsilon \sim \overline{u}^3$
0
1
2
3
Velocity (m s^{-1})

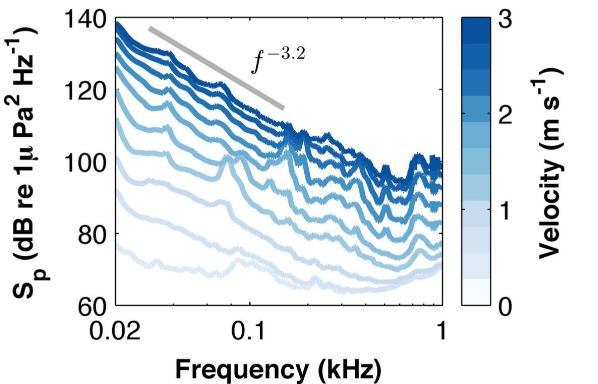

S_p (dB re 1μ Pa^2 Hz^{-1})
140
120
100
80
60
0.02
0.1
1
Frequency (kHz)
$f^{-3.2}$
Velocity (m s^{-1})
3
2
1
0

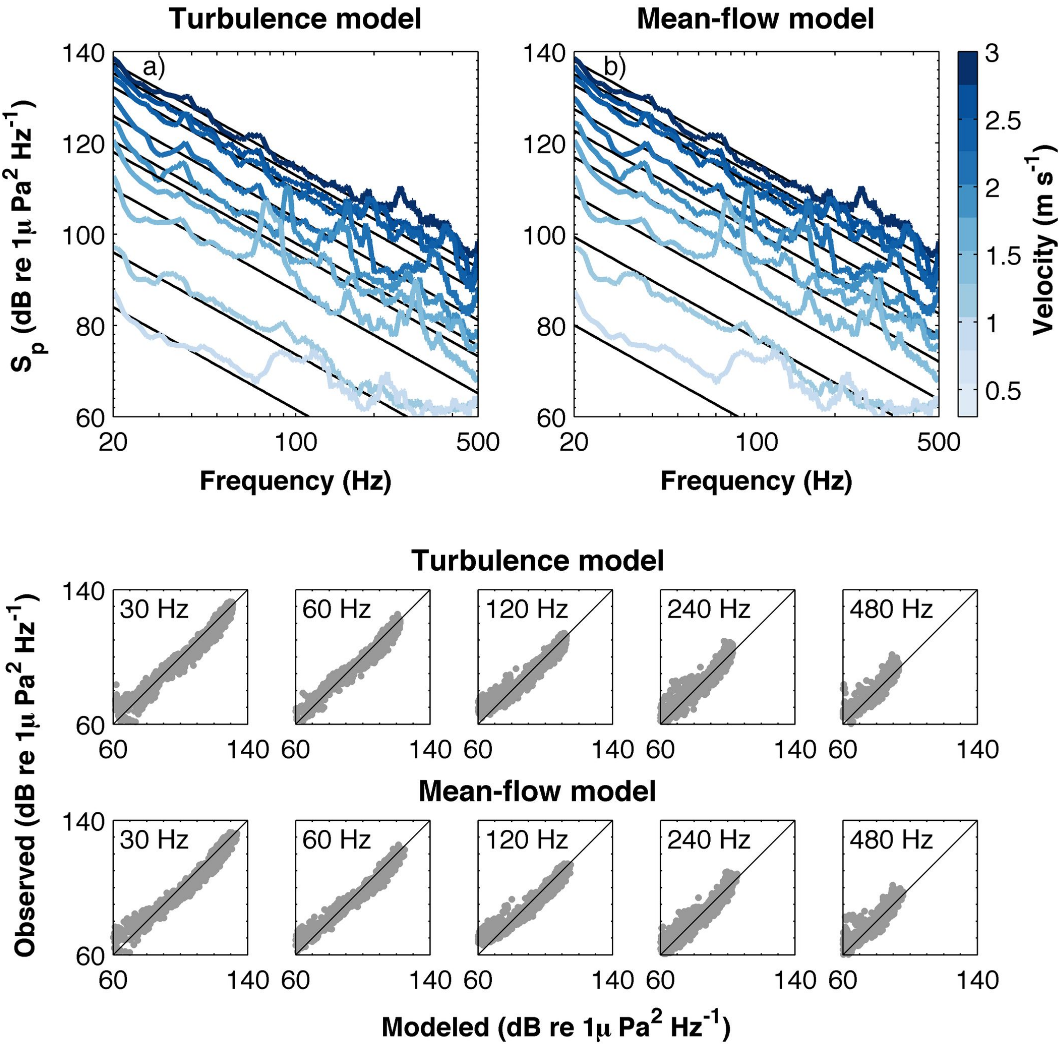

Turbulence model
Mean-flow model
a)
b)
S_p (dB re 1μ Pa^2 Hz^{-1})
Frequency (Hz)
Velocity (m s^{-1})
140
120
100
80
60
20
100
500
3
2.5
2
1.5
1
0.5
Turbulence model
Mean-flow model
30 Hz
60 Hz
120 Hz
240 Hz
480 Hz
Observed (dB re 1μ Pa^2 Hz^{-1})
Modeled (dB re 1μ Pa^2 Hz^{-1})

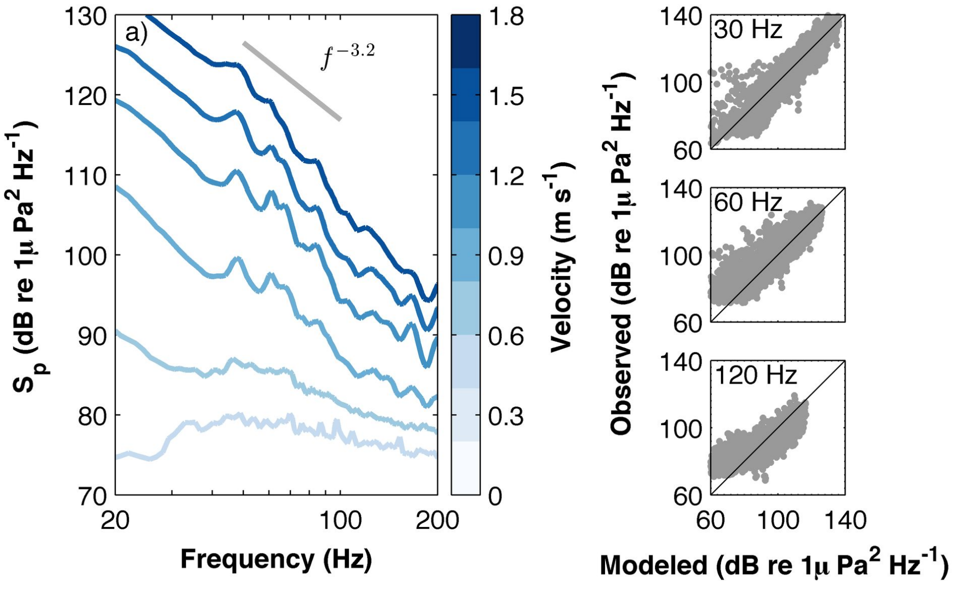

a)
$f^{-3.2}$
130
120
110
100
90
80
70
20
100
200
Frequency (Hz)
S_p (dB re 1μ Pa^2 Hz^{-1})
1.8
1.5
1.2
0.9
0.6
0.3
0
Velocity (m s^{-1})
30 Hz
60 Hz
120 Hz
140
100
60
Observed (dB re 1μ Pa^2 Hz^{-1})
Modeled (dB re 1μ Pa^2 Hz^{-1})